JAERI-M
91-176

ABSOLUTE CALIBRATION OF THE NEUTRON YIELD MEASUREMENT ON JT-60 UPGRADE

October 1991

Takeo NISHITANI, Hiroshi TAKEUCHI, Cris W. BARNES[*1]
Tetsuo IGUCHI[*2], Akira NAGASHIMA, Takashi KONDOH
Akira SAKASAI, Kiyoshi ITAMI, Kenji TOBITA
Keisuke NAGASHIMA, Yuzuru NEYATANI, Yoshihiko KOIDE
Yasunori KAWANO, Shunsuke IDE, Masahiro NEMOTO
Masaaki KURIYAMA, Takao ITOH, Hirotsugu USAMI
Shunsuke KUNIEDA, Jun-ichi KANEKO[*2], Noriaki NAKAYAMADA[*2]
Nobuaki TANAKA[*2], Mamiko SASAO[*3], Takashi SUGIYAMA[*4]
Akiyoshi HATAYAMA[*4], Yoshio KITA[*4], Eiji SEKI[*4] and Yasuo SHIMOMURA

日本原子力研究所
Japan Atomic Energy Research Institute

JAERI-Mレポートは，日本原子力研究所が不定期に公刊している研究報告書です。
入手の問合わせは，日本原子力研究所技術情報部情報資料課（〒319-11茨城県那珂郡東海村）あて，お申しこしください。なお，このほかに財団法人原子力弘済会資料センター（〒319-11 茨城県那珂郡東海村日本原子力研究所内）で複写による実費頒布をおこなっております。

JAERI-M reports are issued irregularly.
Inquiries about availability of the reports should be addressed to Information Division, Department of Technical Information, Japan Atomic Energy Research Institute, Tokai-mura, Naka-gun, Ibaraki-ken 319-11, Japan.

編集兼発行　日本原子力研究所
印　　刷　㈱原子力資料サービス

Absolute Calibration of the Neutron Yield Measurement on JT-60 Upgrade

Takeo NISHITANI, Hiroshi TAKEUCHI, Cris W. Barnes[*1]
Tetsuo IGUCHI[*2], Akira NAGASHIMA, Takashi KONDOH
Akira SAKASAI, Kiyoshi ITAMI, Kenji TOBITA
Keisuke NAGASHIMA, Yuzuru NEYATANI, Yoshihiko KOIDE
Yasunori KAWANO, Shunsuke IDE, Masahiro NEMOTO
Masaaki KURIYAMA[+], Takao ITOH[+], Hirotsugu USAMI[+]
Shunsuke KUNIEDA[+], Jun-ichi KANEKO[*2], Noriaki NAKAYAMADA[*2]
Nobuaki TANAKA[*2], Mamiko SASAO[*3], Takashi SUGIYAMA[*4]
Akiyoshi HATAYAMA[*4], Yoshio KITA[*4], Eiji SEKI[*4]
and Yasuo SHIMOMURA

Department of Fusion Plasma Research
Naka Fusion Research Establishment
Japan Atomic Energy Research Institute
Naka-machi, Naka-gun, Ibaraki-ken

(Received October 1, 1991)

Absolutely calibrated measurements of the neutron yield are important for the evaluation of the plasma peformance such as the fusion gain Q in DD operating tokamaks. Total neutron yield is measured with ^{235}U and ^{238}U fission chambers and ^{3}He proportional counters in JT-60 Upgrade. The in situ calibration was performed by moving the ^{252}Cf neutron source toroidally through the JT-60 vacuum vessel. Detection efficiencies of three ^{235}U and two ^{3}He detectors were measured for 92 locations of the neutron point source in toroidal scans at two different major radii. The total detection efficiency for

+ Department of Fusion Facility
*1 Los Alamos National Laboratory
*2 University of Tokyo
*3 National Institute of Fusion Science
*4 Toshiba Corporation

the torus neutron source was obtained by averaging the point efficiencies over the whole toroidal angle. The uncertainty of the resulting absolute plasma neutron source calibration is estimated to be ± 10%.

Keyword: Neutron Yield, JT-60 Upgrade, Absolute Calibration, Fission Chamber, Deuterium Plasma, Fusion Gain

大電流化JT－60における中性子発生率測定の絶対較正

日本原子力研究所那珂研究所炉心プラズマ研究部
西谷 健夫・竹内 浩・Cris. W. BARNES[*1]
井口 哲夫[*2]・長島 章・近藤 貴・逆井 章
伊丹 潔・飛田 健次・永島 圭介・闍谷 譲
小出 芳彦・河野 康則・井手 俊介・根本 正博
栗山 正明[+]・伊藤 孝雄[+]・宇佐美広次[+]・国枝 俊介[+]
金子 純一[*2]・中山田憲昭[*2]・田中 信彰[*2]・笹尾真実子[*3]
杉山 隆[*4]・畑山 明聖[*4]・北 好夫[*4]・関 英治[*4]
下村 安夫

(1991年10月1日受理)

重水素放電を行うトカマクにおいて，中性子発生量の絶対較正は核融合利得（Q）などのプラズマ性能を評価する上で極めて重要である。大電流化JT－60（JT－60 U）では，^{235}Uと^{238}Uの核分裂計数管および^{3}He比例計数管で中性子発生量の測定を行うが，それに先立ち，^{252}Cf中性子源をJT－60の真空容器内で移動させて中性子検出器のその場較正を行った。まず，磁気軸上の92点において点線源に対する検出効率を測定し，それを平均することによって，トーラス状線源に対する検出効率を求めた。磁気軸の位置としては，JT－60 Uの典型的な磁場配位に対応する2つの位置（R＝3.42 m，3.22 m）で較正を行った。最終的に本較正によって得られる中性子発生量の測定誤差は10％程度と評価された。

那珂研究所：〒311－01 茨城県那珂郡那珂町向山801－1
＋ 核融合装置試験部
＊1 ロスアラモス研究所
＊2 東京大学工学部
＊3 核融合科学研究所
＊4 ㈱東芝

目　　次

Contents

1. Introduction

JT-60 is modified to be tokamak of deuterium plasma with Ip≤7MA and V≤100m^3, which is called JT-60 Upgrade (JT-60U) [1]. The JT-60U physics objective is the study of the reactor-grade plasmas near fusion power break-even, Q≈1, where Q=fusion power/heating power. The fusion neutron yield is most important parameter to estimate Q, because the generated fusion power is proportional to the neutron yield. While the stored energy is used as the bulk parameter of the plasma on the transport analysis, the neutron yield has different sensitivity on certain plasma parameters than the stored energy. For example, it is more sensitive to the deuterium dilution through Z_{eff} of the H/D ratio. Not only the stored energy but also the neutron yield is important on the plasma transport analysis. Of course, neutron yield is necessary in the point of health physics to estimate the device activation, radiation dose, and sky shine problem, etc. Therefor the accuracy of the neutron yield is needed in the DD or DT operational fusion devices.

The absolute calibration of the relation between the neutron source strength in the whole plasma and the output of neutron monitor is a most important problem in the measurements of the neutron yield The calibration is rather difficult because the neutron source is distributed in the plasma which is surrounded with many complicated structures such as first wall, vacuum vessel poloidal and toroidal coils. Many efforts and time are devoted to the calibration at many tokamaks [2-13] An moderated ^{235}U fission chamber is popular for the neutron yield measurement with temporal resolution in large tokamaks such as TFTR and JET. In TFTR [2-6] the calibration of the fission chambers has been performed by moving a ^{252}Cf neutron source, and each DD and DT neutron generator in the vacuum vessel. JET [7-9] has employed the calibration using ^{252}Cf neutron source.

A workshop of the neutron calibration techniques was held on 1-3 August at Princeton discussed possible consensus neutron calibration techniques appropriated to DD plasmas in tokamaks. The workshop recommended two suitable techniques: (1) a ^{252}Cf source calibration of epithermal neutron detectors with a high-sensitive detector,and (2) threshold neutron activation of Ni foil placed vertically or below the plasma. We carried on the ^{252}Cf source calibration of epithermal fission detectors on 4-9 July 1991, according with the recommendation (1). The ``activation calibration'' using three types of material, nickel [^{58}Ni(n,p)^{58}Co] and indium [^{115}In(n,n')^{115}In^{m}] activation foils, and CR-39 track detectors, was carried on simultaneously. The results will be reported elsewhere.

Section 2 describes the neutron detectors and calibration apparatus. Section 3

presents the results of the calculation. The details of the results, and the errors of the calibration and neutron yield are discussed in Section 4.

2. Physical Description of Detectors and Calibration Apparatus

2.1 Detectors

We employed three types of the neutron detector; ^{235}U and ^{238}U fission chambers, and ^{3}He proportional counter. Fission chamber, which is a ionization chamber of which wall is coated by fissile material such as ^{235}U and ^{238}U, is suitable for the neutron yield measurements for the DD plasmas. Energy released by fission is so large, 150 - 200 MeV, that it is easy to reject the effect of γ-ray whose energy is not more than 20 MeV in the DD operational tokamaks. The mean free path of the fission fragment is so short that distance between the anode and cathode can be much shorter than that of other gas counter such as BF_3 chamber. Therefor fission chambers are not so affected by the magnetic field. Large charge generated by the fission enable us to use it in current mode, so the wide range of the neutron flux, typically 9 or 10 decades, can be measured.

The ^{235}U detector is used in the low and medium neutron yield discharges and the ^{238}U detector is used in the high neutron yield discharges such as high-power NB heating experiments. The ^{3}He proportional counter has high detection efficiency. So the detector can obtain sufficient statics in the ^{252}Cf source calibration and plays a role of "temporary detector" to cross-calibrate less sensitive detectors using DD tokamak discharges.

Arrangement of the neutron detectors on the JT-60U is shown in Fig.1. Rate detectors were placed on the torus midplane, just outside the toroidal field coils, at three different toroidal bays out of 18 Bays total: P-3 (next to the ``diagnostic stage'' at Bay P-2); P-7 (between NBI ports that are above and below the midplane); and P-13 (also between NBI ports). At P-3 and P-7 were located one each of a ^{3}He proportional counter, a ^{238}U fission chamber with 1.5 grams, and a ^{235}U fission chamber . At P-13 were another 0.3 gram ^{235}U detector by Toshiba, and another Reuter-Stokes ^{238}U detector, for 8 detectors total. The detector locations and types are summarized in Table 1.

Figures 2 and 3 show the schematics of ^{235}U and ^{238}U detectors, and ^{3}He proportional counter, respectively. The detectors have all long cylinders in geometry. The ^{235}U detector is surrounded 50 mm thick polyethylene of moderator, and 1 mm thick cadmium of thermal neutron shield, whose neutron sensitivity is estimated to be almost constant in the energy range of 0.55 eV to 2.5 MeV. The ^{238}U detector is surrounded by 50 mm thick lead of gamma shield only. The detectors

presents the results of the calculation. The details of the results, and the errors of the calibration and neutron yield are discussed in Section 4.

2. Physical Description of Detectors and Calibration Apparatus

2.1 Detectors

We employed three types of the neutron detector; ^{235}U and ^{238}U fission chambers, and ^{3}He proportional counter. Fission chamber, which is a ionization chamber of which wall is coated by fissile material such as ^{235}U and ^{238}U, is suitable for the neutron yield measurements for the DD plasmas. Energy released by fission is so large, 150 - 200 MeV, that it is easy to reject the effect of γ-ray whose energy is not more than 20 MeV in the DD operational tokamaks. The mean free path of the fission fragment is so short that distance between the anode and cathode can be much shorter than that of other gas counter such as BF_3 chamber. Therefor fission chambers are not so affected by the magnetic field. Large charge generated by the fission enable us to use it in current mode, so the wide range of the neutron flux, typically 9 or 10 decades, can be measured.

The ^{235}U detector is used in the low and medium neutron yield discharges and the ^{238}U detector is used in the high neutron yield discharges such as high-power NB heating experiments. The ^{3}He proportional counter has high detection efficiency. So the detector can obtain sufficient statics in the ^{252}Cf source calibration and plays a role of "temporary detector" to cross-calibrate less sensitive detectors using DD tokamak discharges.

Arrangement of the neutron detectors on the JT-60U is shown in Fig.1. Rate detectors were placed on the torus midplane, just outside the toroidal field coils, at three different toroidal bays out of 18 Bays total: P-3 (next to the ``diagnostic stage'' at Bay P-2); P-7 (between NBI ports that are above and below the midplane); and P-13 (also between NBI ports). At P-3 and P-7 were located one each of a ^{3}He proportional counter, a ^{238}U fission chamber with 1.5 grams, and a ^{235}U fission chamber . At P-13 were another 0.3 gram ^{235}U detector by Toshiba, and another Reuter-Stokes ^{238}U detector, for 8 detectors total. The detector locations and types are summarized in Table 1.

Figures 2 and 3 show the schematics of ^{235}U and ^{238}U detectors, and ^{3}He proportional counter, respectively. The detectors have all long cylinders in geometry. The ^{235}U detector is surrounded 50 mm thick polyethylene of moderator, and 1 mm thick cadmium of thermal neutron shield, whose neutron sensitivity is estimated to be almost constant in the energy range of 0.55 eV to 2.5 MeV. The ^{238}U detector is surrounded by 50 mm thick lead of gamma shield only. The detectors

were oriented vertically and place just beyond the outer diameter of the toroidal field coils to reduce the effects of the magnetic fields. Being in line with midplane ports, the detectors had a minimum of shielding between themselves and the plasma neutrons The triplets or pairs of detectors at each Bay spanned most of the breadth of the Bay, leading to significant differences in the sightlines for streaming neutrons to each detector .

We use ^{235}U and ^{238}U fission chambers in both pulse counting mode and Campbell (MSV) mode, former is suitable for low count rate less than 10^6 cps and later is for high count rate more than 10^5 cps. A pair of the ^3He detector are operated in pulse counting mode only.

2.2 The Calibration Source Transfer System

A remotely controlled source transfer system positioned the neutron point source in the vacuum vessel of JT-60 U. The source transfer system consisted of `train and track" is shown as shown in Fig.4. The ^{252}Cf source was lowered by a fishing line into a funnel into a vertical pipe where it was supported at a height 15 cm above the midplane of the torus (corresponding to the height of the magnetic axis for the lower-divertor plasmas of JT-60U). The pipe was then mounted on a flat ``train" that drove around a ``track" mounted inside the vacuum vessel (see Fig. 5). Actually the train was more like a moon rover car that travelled a road, with the car about 2 feet long and one foot wide. The source pipe was at one end of the car, and a TV camera was at the other end, with a broadcast unit mounted in the middle of the car. The road had an inverted ridge that the car steered along. Power was obtained from a 12 Volt power bar running toroidally around the vessel inside and somewhat above the road. The source pipe could be placed at two radial locations, corresponding to 3.42 m and 3.22 m major radius (typical equilibrium positions of the magnetic axis for standard and high elongated configurations, respectively). Most of the mass of the train and track was located below the midplane. The TV signal was broadcast out of the vacuum vessel to a receiver in the adjacent clean room, and then piped by wire into the diagnostic control room where a digital clock was added to the signal and recorded on a VTR. One of the significant concerns of the calibration was the un-quantified effect on neutron scattering of the significant amount of mass in the calibration apparatus.

The track was labelled every 0.5^o with the toroidal angle from the center of Bay P-1 (the entrance port) of the source when the TV camera was looking at the label. The calibration was done point by point by moving the car to an angle, stopping, and counting for 1000 seconds (with a few points for 2000 seconds). The last 18 hours of calibration were an attempt to calibrate activation and track

detectors, with the car kept in constant toroidal motion. A test was performed before the calibration, tabulating the digital time from the VTR tape of the camera motion, to check the constancy of the angular velocity of the car. The test revealed some systematic variation with angle at about 3% RMS deviation (see Fig. 6), but the variation changes sign rapidly enough to cause less than a 0.3% effect on the integrated calibration.

In addition to the usual line efficiency calibration, point calibrations of the neutrons coming from the neutral beam ion dumps and calorimeter were done. This was achieved by placing the source down a funnel and pipe installed in the beam box at Bay P-7.

2.3 ^{252}Cf Source

The ^{252}Cf source of 400 MBq manufactured by Amersham was used here. It had a calibrated source strength of 5.14×10^7 n/sec on March 25, 1991, and had decayed (with an assumed half-life of 966.1 days) to 4.78×10^7 n/sec by July 4 when the calibration began. The intensity remained constant during 5 days duration of the calibration. The ^{252}Cf source was sealed by stainless steel capsule of 7.8 mm diam. × 10 mm height. The angular emission is isotropic. the energy spectrum can be represented by a simple Maxwellian distribution of the form,

$$N(E) = CE^{1/2} \exp(-\frac{E}{T})$$

where T is a residual nuclear temperature of 1.42 MeV. The averaged neutron energy is 2.14 MeV, which is near 2.45 MeV for the DD neutron energy.

2.4 Data Acquisition

All eight detector signals were acquired into a LeCroy 8590 scaler under computer CAMAC control. However, the data was summed into only one time bin; also, with 16 bit counters the data from the ^{3}He detectors overflowed at 2^{16}=65536 counts. The data from all the detectors except the ^{238}U ones were also acquired onto 6-digit manual scalers. Finally, because of ``noise'' in one of the Toshiba ^{235}U detectors (see below) after the first few data points the signal from that detector was also acquired onto a stand-alone multi-time-bin scaler unit. The triggering of the computer, stand-alone scaler,and manual scalers was manual, with a count down used to synchronize the three buttons to be pushed. All three of the sets of numbers (CAMAC , manual scalers, and stand-alone scaler values) were tabulated. The manual synchronization worked well enough, with good agreement between the various tabulations.

3. Calibration Results

3.1 Detector Efficiencies for Point Source

The counts of the detectors for point neutron source are shown in Table 2. Not only high-sensitive ^{3}He detector but also 0.3 g ^{235}U detectors have sufficient statistical certainty. The point efficiencies, counts per neutron from a point at a single angle, of the detectors at Bay P3 and P7 are shown Fig. 7 and 8, respectively. The noise of the detectors at Bay P3 and P7 is quite low, so that meaningful data was obtained for the point source opposite side of the detectors. While we suffered from noise at low count rates in Bay P13 detectors, nearly identical to the problems that were reported on TFTR. The Bay P-13 ^{238}U fission chamber was very noisy and useless; the other ^{238}U detectors had a constant background rate that may be able to be subtracted, allowing a direct, albeit inaccurate, calibration of them. The primary problem was with the Bay P-13 ^{235}U detector, which had clear count spikes (say 50 at a time when the usual rate was only 1) but also possible lower level values of noise. The detector was monitored with the stand-alone scaler, and "noise" counts were subjectively determined, tabulated, and thrown out. The count rate was well above the noise level at the peak angles in the calibration, and even using the raw uncorrected data does not change the line efficiency calculation very much. Figure 9 illustrates the difference between the raw and ``corrected'' net counts in this detector.

3.2 Detector Efficiencies for Toroidal Line Source

The point efficiencies can be integrated and averaged with angle to provide toroidal line efficiencies. Multiple data points at a single angle are first averaged together; the integrals using a simple Simpson's rule a cubic spline fit do not differ. The obtained toroidal line efficiencies are summarized in Table. 3. The data from the two major radii are very similar, with a typical reduction of only 2% for the 20 cm difference.

The ratio of efficiencies of the three ^{235}U detectors are not proportional to the difference in fissionable mass. The Toshiba 0.3 gram detectors are more sensitive per gram than the 1.5 gram Reuter-Stokes detector, and the observed factor of 3 ratio in the line efficiencies is close to the predicted neutron sensitivity ratio of 3.5 from lab tests.

The toroidal line efficiencies could also be obtained from the constant revolution of the source during the activation calibration. During a 1160 second revolution (16 turns) the scalers could be triggered, and over 9000 counts obtained in

the 0.3 gram ^{235}U detectors (and about 1×10^6 in the ^3He detectors). The resulting line efficiencies were indentical to the integrated point efficiencies, except the noisy $^{235}U3$ detector..

4. Discussions

4.1 Details of the Point Efficiencies

The advantage of taking the point efficiency data does not lie in increased accuracy compared to the constant revolution method, but in the ability to see and understand more of the details and hence evaluate the uncertainties better. Figures 10 and 11 show the point efficiencies for the ^3He and ^{235}U detectors in Bay P-3, with the ^{235}U data multiplied by 60 to place it on the same scale. The details of this data can all be explained: the very low values at large angles as the source is behind the center core; the sharp drop of the ^{235}U data at 155° as the source comes from behind the shadow of the central core, and neutrons with high energy directly stream to it; the sharp increase in efficiency as the source appears from behind the TF coils of the Bay; the angular shifts of the data because of the different toroidal position in the Bay; and the "three" peaks in the data as the neutrons stream first through one camera port, then between the flanges, and then through the second port, at just the correct geometric angles (the third "peak" at 15° is actually absent, due to the actual presence of a large bake-out valve in front of the ^3He detector in the Bay).

The neutron calibration of TFTR shows that a good approximation to calibration data can be achieved using fits that are exponential in angle. Figure 12 shows such a semi-log plot, illustrating on JT-60U that the data clearly is curved on this plot and not exponential. Also, the shift in angle due to the asymmetry of the port box structure is clearly apparent when plotted versus the absolute value of the angle.

4.2 Comparison with the MCNP Calculation

Figure 13 shows the comparison of the point efficiencies between the experiment and the MCNP[14] calculation[15] for the ^{235}U-1 of Bay P-3. The point efficiency of the calculation was normalized to that of the experiment at 0°, because the *nv* efficiency of the actual detectors was unknown. The toroidal line efficiency is 6.6×10^{-8} counts/(source neutron), which is 24% larger than that of experiment. The MCNP calculation has symmetry in the modeling of JT-60 U, while the actual machine, especially port box in front of the detector, has asymmetry. The experimental point efficiencies in the range 0° ~ +180° have good agreement with the calculation, while those in the range 0° ~ -180° are smaller than the calculation.

the 0.3 gram ^{235}U detectors (and about 1×10^6 in the ^3He detectors). The resulting line efficiencies were indentical to the integrated point efficiencies, except the noisy $^{235}U3$ detector..

4. Discussions

4.1 Details of the Point Efficiencies

The advantage of taking the point efficiency data does not lie in increased accuracy compared to the constant revolution method, but in the ability to see and understand more of the details and hence evaluate the uncertainties better. Figures 10 and 11 show the point efficiencies for the ^3He and ^{235}U detectors in Bay P-3, with the ^{235}U data multiplied by 60 to place it on the same scale. The details of this data can all be explained: the very low values at large angles as the source is behind the center core; the sharp drop of the ^{235}U data at 155° as the source comes from behind the shadow of the central core, and neutrons with high energy directly stream to it; the sharp increase in efficiency as the source appears from behind the TF coils of the Bay; the angular shifts of the data because of the different toroidal position in the Bay; and the "three" peaks in the data as the neutrons stream first through one camera port, then between the flanges, and then through the second port, at just the correct geometric angles (the third "peak" at 15° is actually absent, due to the actual presence of a large bake-out valve in front of the ^3He detector in the Bay).

The neutron calibration of TFTR shows that a good approximation to calibration data can be achieved using fits that are exponential in angle. Figure 12 shows such a semi-log plot, illustrating on JT-60U that the data clearly is curved on this plot and not exponential. Also, the shift in angle due to the asymmetry of the port box structure is clearly apparent when plotted versus the absolute value of the angle.

4.2 Comparison with the MCNP Calculation

Figure 13 shows the comparison of the point efficiencies between the experiment and the MCNP[14] calculation[15] for the ^{235}U-1 of Bay P-3. The point efficiency of the calculation was normalized to that of the experiment at 0°, because the *nv* efficiency of the actual detectors was unknown. The toroidal line efficiency is 6.6×10^{-8} counts/(source neutron), which is 24% larger than that of experiment. The MCNP calculation has symmetry in the modeling of JT-60 U, while the actual machine, especially port box in front of the detector, has asymmetry. The experimental point efficiencies in the range 0° ~ +180° have good agreement with the calculation, while those in the range 0° ~ -180° are smaller than the calculation.

4.3 Preliminary Calibration of the ^{238}U detector

The ^{238}U detectors are not very sensitive, but they did see an observable peak in their point efficiency. A single 3 hour point was taken of this detector in the center of Bay P-3 (arrow and label on Figure 14). By the integration of the point efficiencies, the toroidal line efficiency of 8.5×10^{-11} counts/(source neutron) was obtained. The efficiency is about twice larger than that provided from the cross-calibration between ^{238}U and ^{235}U detectors using tokamak discharges. More care will need to be taken in doing the background subtraction and angular integral to get a believable number; more importantly, the energy sensitivity of the ^{238}U detectors makes a ^{252}Cf calibration not applicable directly to DD plasmas. If the more precise modelling is made, the MCNP calculation will be useful in the estimation of the efficiency.

4.4 Cross Calibration of ^{235}U Detectors between Pulse Counting and MSV modes.

Neutral beam experiments are mainly interested in JT-60 Upgrade. In those experiments, the neutron yield exceeds 10^{14} n/s, where the pulse counting mode is not available due to pulse pile-up. In the range of neutron yield, we have to use Campbell mode or current mode. Campbell mode is employed for the high neutron yield in JT-60 Upgrade. The intensity of our ^{252}Cf source is too low to calibrate the fission chamber in Cambelling directly. So the cross calibration of the ^{235}U detector from the pulse counting mode to the Campbell mode was performed during the ohmically heated tokamak discharges in the rage of neutron yield 10^{11} - 10^{13} n/s, where the Campbell signal overlaps the pulse counting signal. Good linearity between the pulse counting and Campbell modes was obtained in the range of the neutron yield as shown in Fig.15. Above the neutron yield of 10^{13} n/s, the count rate was saturated by the pulse pile-up and the dead time of the electronics. The standard deviation between the pulse counting and Campbell modes was 5% including the Fractuation of the Campbell electronics.

4.5 Measurement Uncertainties for Neutron Yield

The sources of the calibration and measurement uncertainties are listed in Table 4, where uncertainties by the calibration hardware scattering, and the energy difference between ^{252}Cf and DD neutrons are estimated by the MCNP calculations[15]. The linearity of the Campbell mode was investigated using a fission reactor by changing the output power step by step. The The total uncertainties are derived from the root-mean-square of each source uncertainty. The expected uncertainties in the neutron yield measurement are 10% for the pulse count mode

(Sn ≤ 10^{13} n/s) and 11% for the Campbell mode (Sn ≥ 10^{12} n/s).

Acknowledgements

The authors would like to thank Mr. M. Yamamoto for his effort to the installation of the calibration train and track in the vacuum vessel. The continuing supports of Drs. S. Tamura, H. Kishimoto, A. Kitsunezaki and M. Nagami.

(Sn ≤ 10^{13} n/s) and 11% for the Campbell mode (Sn ≥ 10^{12} n/s).

Acknowledgements

The authors would like to thank Mr. M. Yamamoto for his effort to the installation of the calibration train and track in the vacuum vessel. The continuing supports of Drs. S. Tamura, H. Kishimoto, A. Kitsunezaki and M. Nagami.

References

[1] M. Kikuchi, T. Ando, M. Araki, T. Horie, H. Horiike, Y. Ikeda, H. Kishimoto, K. Koizumi, M. Matsukawa, T. Matsukawa, Y. Neyatani, H. Ninomiya, T. Nishitani, S. Seki, H. Takatsu, M. Yamamoto, in Symp. on Fusion Technol. 1988, 9Utrecht, 1988) p287.

[2] E. B. Nieschmidt, A. C. England, H.W. Hendel, J. A. Isaacson, L. P. Ku, F. Y. Tsang, Rev. Sci. Instrum. **56** (1985) 1084.

[3] H. W. Hendel, D. L. Jassby, H. S. Bosch, Cris. W. Barnes, L. C. Johnson, T. J. Murphy, E. B. Nieschmidt, T. Saito,J. D. Strachan, G. D. Tait,K. M. Young, Rev. Sci. Instrum. **59** (1988) 1682.

[4] E. B. Nieschmidt, T. Saito, C. W. Barnes, H.-S. Bosch, T. J. Murphy, Rev. Sci. Instrum. **59** (1988) 1715.

[5] H.-S. Bosch, J. D. Strachan, Cris W. Barnes, E. B. Nieschmidt, Rev. Sci. Instrum.. **59** (1988) 1718.

[6] H.W. Hendel, R.W. Palladino, Cris W. Barnes, N. Diesso, J.S. Felt, D.L. Jassby, L.C. Johnson, L.-P. Ku, Q.P. Liu, R.W. Motley, H.B. Murphy, J. Murphy, E.B. Nieschmidt, J.A. Roberts, T. Saito, J.D. Strachan, R.J. Waszazak, K.M. Young, Rev. Sci. Instrum. **61** (1990) 1900.

[7] O. N. Jarvis, J. Källne, G. Sadler, P. van Belle, K. H. Beimer, T. Elevant, A. R. Talbot, JET Report, JET-IR(84)02 (1984).

[8] O. N. Jarvis, J. Källne, G. Sadler, P. van Belle, M Hone, M. Merlo, E. W. Lees, M. T. Swinhoe, A. R. Talbot, A. H. Armitage, JET Report, JET-IR(85)06(1984).

[9] O.N. Jarvis, G. Sadler, P. van Bell, T. Elevant, Rev. Sci. Instrum. **61** (1990) 3172.

[10] G. Zankel, J. D. Strachan, R.Lewis, W. Pettus, J. Schmotzer, Nucl. Instrum. Methods **185** (1981) 321.

[11] K. Hübner,et al., in 16th Europ. Conf. on Controlled Fusion and Physics, (Venice,1989) part 4, p1453.

[12] M. Angelone, P. Batistoni, L. Bertalot, B. Esposito, M. Martone, M. Pillon, S. Podda, M. Rapisardam S. Pollet, Rev. Sci. Instrum. **61** (1990) 3157.

[13] C.L. Fiore, R.S. Grenetz, Rev. Sci. Instrum. **61** (1990) 3166.

[14] "MCNP MonteCarlo Neutron and Photon Transport Code", Ork Ridge National Laboratory, CCC-200 (1983).

[15] T. Nishitani, "Monte Carlo Simulation for the Calibration of Neutron Source Strength MEasurement of JT-60 Upgrade", JAERI-M 89-138, (1989).

Table 1 Neutron detectors, locations, Fissionable materials, and types

Detector	Location	Fissionable material	Mass	Type	
^{235}U1	P-3	^{235}U	1.5g	Reuter Stokes	NA-04
^{235}U2	P-7	^{235}U	0.3g	Toshiba	KSA-01
^{235}U3	P-13	^{235}U	0.3g	Toshiba	KSA-01
^{238}U1	P-3	^{235}U	1.5g	Reuter Stokes	RS-C3-2410-102
^{238}U2	P-7	^{235}U	1.5g	Reuter Stokes	RS-C3-2410-102
^{238}U3	P-13	^{235}U	1.5g	Reuter Stokes	RS-C3-2410-102
^{3}He1	P-3	^{3}He		20th Century	31He^{3}/380/25B
^{3}He3	P-3	^{3}He		20th Century	31He^{3}/380/25B

Table 3 Detector efficiencies for toroidal line source

	Line efficiencies (counts/ source neutron)		
	Integration of point efficiencies		Constant revolution
Detector	R= 3.42 m	R = 3.22 m	R = 3.42 m
^{235}U1	5.34×10^{-8}	5.26×10^{-8}	5.34×10^{-8}
^{235}U2	1.78×10^{-8}	1.74×10^{-8}	1.78×10^{-8}
^{235}U3	1.92×10^{-8}	1.88×10^{-8}	(2.09×10^{-8})*
^{3}He1	3.27×10^{-6}	3.22×10^{-6}	3.27×10^{-6}
^{3}He3	2.83×10^{-6}	2.78×10^{-6}	2.83×10^{-6}

* Including noise counts

Table 2(a) Counts of detectors for point source (R=3.42m)

Toroidal Angle	Time (s)	Scaler 1	Scaler 2	Scaler 3	Scaler 4	Scaler 5	Multi Bin Scaler (U235 P13)		
degree		U235 P3	U235 P7	U235P13	He3 P3	He3 P7	Raw	Noise	Net
0.0	1000	2544	100	239	166432	19124			
0.0	1000	2534	111	156	166281	19298	157	36	121
5.0	1000	3116	167	113	200938	36064			
5.0	1000	3011	144	208	200758	36227	214	99	115
10.0	1000	3792	212	164	246233	37900			
10.0	1000	3719	213	147	246809	37908	154	73	81
15.0	1000	4664	254	130	288668	48231			
15.0	1000	4673	247	170	288360	48530	176	87	89
20.0	1000	5685	262	149	357949	52569			
25.0	1000	7129	304	209	474210	53508		178	
27.5	1000	8029	314	123	513641	55110		77	
30.0	1000	9538	328	81	584972	56533		23	
31.5	1000	9514	361	111	758515	58168	111	52	59
32.5	1000	10213	303	181	857328	58956	195	149	46
34.0	1000	12582	353	148	913158	60595	151	92	59
35.0	1000	13408	357	162	1001807	61296	166	113	53
36.5	1000	13715	346	138	1066988	63127	148	97	51
37.5	1000	15062	403	161	936845	64164	170	118	52
39.0	1000	16711	421	123	933385	66040	130	86	44
40.0	1000	15729	404	145	924864	67305	150	109	41
41.5	1000	16516	375	100	992166	68044	106	68	38
42.5	1000	16950	409	97	1040045	70436	100	55	45
44.0	1000	15476	395	99	1037253	72097	101	52	49
45.0	1000	15591	461	101	1013244	73284	105	68	37
46.5	1000	15771	426	75	893533	75964	77	40	37
47.5	1000	16144	405	80	832010	78278	83	51	32
50.0	1000	13963	493	106	802258	83223	111	51	60
52.5	1000	12054	513	94	777142	88216	98	62	36
55.0	1000	12344	539	145	782358	93120	145	112	33
57.5	1000	11835	572	72	641780	98223	75	27	48
60.0	1000	11054	601	126	495369	104290	132	85	47
65.0	1000	7349	687	86	381219	117068	87	48	39
70.0	1000	5305	772	76	313963	133852	77	36	41
75.0	1000	4123	934	84	263089	153867	88	46	42
80.0	1000	3589	1011	101	223940	182148	105	64	41
85.0	1000	3013	1317	86	191934	215927	88	37	51
90.0	1000	2629	1608	157	166190	260624	163	108	55
95.0	1000	2313	1936	147	144569	355592	153	86	67
100.0	1000	2027	2646	166	127541	416340	172	115	57
105.0	1000	1869	3433	91	112687	657963	91	29	62
107.5	1000	1705	4451	113	105741	720992	114	39	75
110.0	1000	1638	4750	167	99869	769271	179	95	84
112.5	1000	1526	5039	164	93940	830431	171	91	80
115.0	1000	1452	5344	133	88370	880925	134	51	83
117.5	1000	1317	5510	159	83380	856224	170	62	108
120.0	1000	1308	5774	200	79325	762175	202	81	121
122.5	1000	1264	5355	163	75590	702379	166	56	110
125.0	1000	1194	4897	206	73101	654514	211	81	130
127.5	1000	1184	4031	226	70219	587785	231	101	130
130.0	1000	1139	3646	285	66307	506921	293	85	208
132.5	1000	1105	3158	274	63740	453331	275	41	234
135.0	1000	1113	2668	277	61650	412505	281	32	249
140.0	1000	1031	2124	292	55919	341822	293	36	257

Table 2(a) (continued)

Toroidal Angle	Time (s)	Scaler 1	Scaler 2	Scaler 3	Scaler 4	Scaler 5	Multi Bin Scaler (U235 P13)		
degree		U235 P3	U235 P7	U235P13	He3 P3	He3 P7	Raw	Noise	Net
145.0	1000	944	1739	414	50083	278557	421	88	333
150.0	1000	976	1489	419	41832	231884	420	84	336
155.0	1000	917	1243	409	34258	195694	414	41	373
160.0	1000	413	1063	458	24681	165122	464	82	382
165.0	1000	356	851	525	21107	141568	528	89	439
170.0	1000	326	773	630	18408	122077	636	141	495
175.0	1000	264	719	634	15072	106346	635	87	548
180.0	1000	226	547	655	13214	93736	664	72	592
185.0	1000	186	534	775	11494	82510	783	115	668
190.0	1000	200	452	795	10388	73833	822	50	772
195.0	1000	148	427	945	9414	66828	962	48	914
200.0	1000	161	366	1090	8735	61687	1125	64	1061
205.0	1000	115	363	1274	7895	56353	1303	79	1224
210.0	1000	143	320	1505	7317	51222	1542	28	1514
215.0	1000	119	304	1856	6989	47642	1860	76	1784
220.0	3000	331	796	7174	20667	128745	7189	264	6925
225.0	1000	120	231	3028	6793	36762	3026	33	2993
227.5	1000	128	205	3878	6658	33120	3869	40	3829
230.0	3000	333	570	15013	20546	85398	15013	90	14923
232.5	1000	122	161	5625	6853	24904	5611	44	5567
235.0	1000	123	147	6192	6934	22001	6191	62	6129
237.5	1000	123	126	6359	7005	20510	6356	150	6206
240.0	3000	347	305	18598	21273	56550	18595	218	18377
242.5	1000	120	89	5991	7517	17072	5988	112	5876
245.0	1000	120	105	5879	7753	15456	5884	117	5767
247.5	1000	127	89	5819	7939	14524	5817	36	5781
250.0	3000	396	254	16168	25106	40127	16172	252	15920
252.5	1000	140	75	4226	8589	12186	4219	29	4190
255.0	1000	130	72	3128	9213	11486	3126	53	3073
260.0	3000	474	195	7986	30507	29492	8011	279	7732
265.0	1000	189	62	2007	11397	8852	2013	53	1960
270.0	3000	601	147	5047	39858	23699	5058	223	4835
275.0	1000	256	44	1413	15554	7315	1416	68	1348
280.0	1000	281	42	1191	18922	6671	1198	69	1129
280.0	2000	596	82	2270	37093	13469	2273	81	2192
285.0	1000	345	47	1021	22861	6252	1024	56	968
290.0	1000	466	47	908	30187	5923	915	90	825
290.0	2000	966	67	1873	60936	12026			0
295.0	1000	644	37	713	39351	5688	714	41	673
300.0	1000	720	34	625	45412	5778	626	37	589
300.0	2000	1350	77	1480	90183	11290			0
305.0	1000	719	29	557	50525	5990	558	22	536
310.0	1000	844	44	489	55137	6069	488	32	456
310.0	2000	1721	68	1029	110768	12022			0
315.0	1000	868	32	473	58971	6423	475	38	437
320.0	1000	999	44	479	64285	6959	484	84	400
325.0	1000	1064	50	449	68936	7392	455	78	377
330.0	1000	1208	56	500	75945	8226	509	140	369
335.0	1000	1311	58	380	84873	9104	390	88	302
340.0	1000	1510	72	410	94753	10293	419	136	283
345.0	1000	1717	88	311	107749	12025	317	82	235
350.0	1000	1976	73	245	122995	13747	250	46	204
355.0	1000	2185	88	176	142300	16091	175	37	138

Table 2(b) Counts of detectors for point source (R=3.22m)

Toroidal Angle	Time (s)	Scaler 1	Scaler 2	Scaler 3	Scaler 4	Scaler 5	Multi Bin Scaler (U235 P13)		
degree		U235 P3	U235 P7	U235P13	He3 P3	He3 P7	Raw	Noise	Net
0.0	1000	2825	114	185	182418	18401	189	80	109
5.0	1000	3284	146	126	214129	22091	128	43	85
10.0	1000	3962	175	191	249555	37528	192	110	82
15.0	1000	4801	230	116	299395	43916	119	31	88
20.0	1000	5678	272	102	367459	54441	106	42	64
25.0	1000	6824	298	91	448177	58267	112	44	68
27.5	1000	7898	324	104	496376	59128	131	57	74
30.0	1000	8206	361	191	655964	59928	218	134	84
31.5	1000	8858	362	87	757171	60396	88	32	56
32.5	1000	9974	356	138	795500	61136	148	99	49
34.0	1000	11606	365	67	862039	62149	69	23	46
35.0	1000	11858	344	81	943258	63722	84	48	36
36.5	1000	12463	389	96	876945	65558	99	56	43
37.5	1000	13745	411	130	807314	67016	136	92	44
39.0	1000	14838	416	226	833310	67965	255	205	50
40.0	1000	14292	414	108	827394	69134	113	78	35
41.5	1000	14268	401	154	887725	70973	162	131	31
42.5	1000	14927	429	162	925960	73013	174	127	47
44.0	1000	14512	442	72	933011	75002	77	38	39
45.0	1000	13925	460	77	928363	76151	78	40	38
46.5	1000	13914	454	64	856222	78841	65	25	40
47.5	1000	14037	458	119	791672	80071	123	89	34
50.0	1000	14075	489	149	732500	83943	162	122	40
52.5	1000	11401	562	78	763797	88581	79	53	26
55.0	1000	10931	558	90	692675	94291	94	51	43
60.0	1000	10609	588	129	570918	109373	139	97	42
65.0	1000	8599	684	111	392201	125640	116	83	33
70.0	1000	6099	816	106	326238	144916	109	73	36
75.0	1000	4759	1016	67	274791	168559	68	26	42
80.0	1000	3832	1166	73	233005	196698	74	36	38
85.0	1000	3286	1405	139	199859	232131	156	110	46
90.0	1000	2823	1696	177	172263	303420	181	125	56
95.0	1000	2477	2064	98	148235	348938	99	39	60
100.0	1000	2186	2569	147	129646	539491	156	101	55
105.0	1000	1841	3730	207	112154	627796	227	156	71
107.5	1000	1715	3970	161	105191	655358	167	95	72
110.0	1000	1605	4434	118	99555	697113	118	38	80
112.5	1000	1531	4512	138	94244	743481	144	67	77
115.0	1000	1521	4644	141	89375	772465	146	53	93
117.5	1000	1382	4874	134	85412	731971	135	34	101
120.0	1000	1440	5109	141	81675	668335	142	44	98
122.5	1000	1278	4884	212	77811	628668	217	101	116
125.0	1000	1283	4581	251	74317	617884	252	96	156
127.5	1000	1256	4172	262	69861	530671	272	120	152
130.0	1000	1202	3239	181	67221	489827	183	20	163
132.5	1000	1210	3132	303	64777	436975	309	96	213
135.0	1000	1049	2684	270	61083	399847	273	62	211
140.0	1000	1089	2103	295	55728	334953	299	48	251
145.0	1000	1038	1823	477	47527	286605	487	214	273
150.0	1000	1004	1528	457	38576	237375	472	155	317
152.5	1000	945	1425	406	34856	217570	410	45	365
155.0	1000	576	1196	486	30658	201729	498	139	359

Table 2(b) (continued)

Toroidal Angle	Time (s)	Scaler 1	Scaler 2	Scaler 3	Scaler 4	Scaler 5	Multi Bin Scaler (U235 P13)		
degree		U235 P3	U235 P7	U235P13	He3 P3	He3 P7	Raw	Noise	Net
160.0	1000	426	1043	412	23575	170525	415	53	362
165.0	1000	359	928	473	20555	145330	473	65	408
170.0	1000	314	766	440	17314	124580	440	23	417
175.0	1000	265	687	621	14693	107407	624	78	546
180.0	1000	233	586	703	12820	93837	706	92	614
185.0	1000	188	508	764	11576	83290	766	62	704
190.0	1000	158	457	877	10128	76013	881	71	810
195.0	1000	170	433	968	9458	68367	970	43	927
200.0	1000	135	407	1219	8365	62113	1226	107	1119
205.0	1000	125	358	1315	7844	57161	1338	101	1237
210.0	1000	112	336	1682	7267	52371	1691	115	1576
215.0	1000	127	288	1933	6895	47496	1934	57	1877
220.0	1000	112	269	2402	6828	41983	2408	60	2348
225.0	1000	121	212	3166	6658	33680	3172	82	3090
227.5	1000	120	175	4145	6655	29026	4154	73	4081
230.0	1000	110	131	4803	6683	25204	4810	112	4698
232.5	1000	122	130	5367	6787	22809	5377	82	5295
235.0	1000	110	120	5432	6828	21159	5430	36	5394
237.5	1000	110	136	5625	7039	19097	5633	139	5494
240.0	1000	131	104	5425	7306	17582	5436	34	5402
242.5	1000	114	91	5219	7422	16356	5220	99	5121
245.0	1000	139	83	5456	7757	15020	5460	40	5420
247.5	1000	123	90	5274	7928	13770	5278	82	5196
250.0	1000	131	96	5055	8193	12720	5056	30	5026
252.5	1000	136	61	4638	8580	11736	4644	35	4609
255.0	1000	133	58	3478	9094	10952	3481	63	3418
260.0	1000	152	47	2573	10149	9716	2578	107	2471
265.0	1000	191	65	2207	11209	8676	2220	134	2086
270.0	1000	192	48	1729	12657	7813	1737	64	1673
275.0	1000	236	48	1504	14867	7097	1511	89	1422
280.0	1000	289	38	1274	17551	6541	1277	103	1174
285.0	1000	333	35	1048	21161	6252	1054	49	1005
290.0	1000	421	35	885	26144	5942	885	7	878
295.0	1000	584	37	842	35646	5683	856	130	726
300.0	1000	680	32	756	44539	5832	762	71	691
305.0	1000	820	37	628	50135	5845	628	45	583
310.0	1000	834	36	593	55704	6129	601	58	543
315.0	1000	908	27	497	61528	6476	503	54	449
320.0	1000	1015	41	511	66892	6988	516	105	411
325.0	1000	1089	41	422	71965	7563	428	71	357
330.0	1000	1205	42	367	78692	8299	371	39	332
335.0	1000	1325	57	356	86542	9061	362	56	306
340.0	1000	1566	67	421	97564	10174	430	134	296
345.0	1000	1736	52	286	111883	11549	294	45	249
350.0	1000	1940	77	268	130207	13446	275	91	184
355.0	1000	2327	79	220	151987	15498	225	88	137

Table 4 Measurement uncertainties for neutron yield

Calibration uncertainty	± 9.9%
^{252}Cf source intensity	± 1.5 %
Statical error	± 0.3 %
Calibration hardware scattering	± 5 %
Energy difference between Cf and DD	± 6 %
Neutron source profile	± 5.5 %
Plasma position variation	± 2%
Neutron yield by pulse counting mode ($Sn \leq 10^{13}$ n/s)	± 10.3%
Calibration uncertainty	± 9.9 %
Statical error (10^5 cps, 10 ms sampling)	± 3 %
Neutron yield by Campbell mode ($Sn \geq 10^{12}$ n/s)	± 11.1%
Calibration uncertainty	± 9.9 %
Cross calibration pulse counting to Campbell mode	± 5 %
Campbell mode linearity	± 1 %

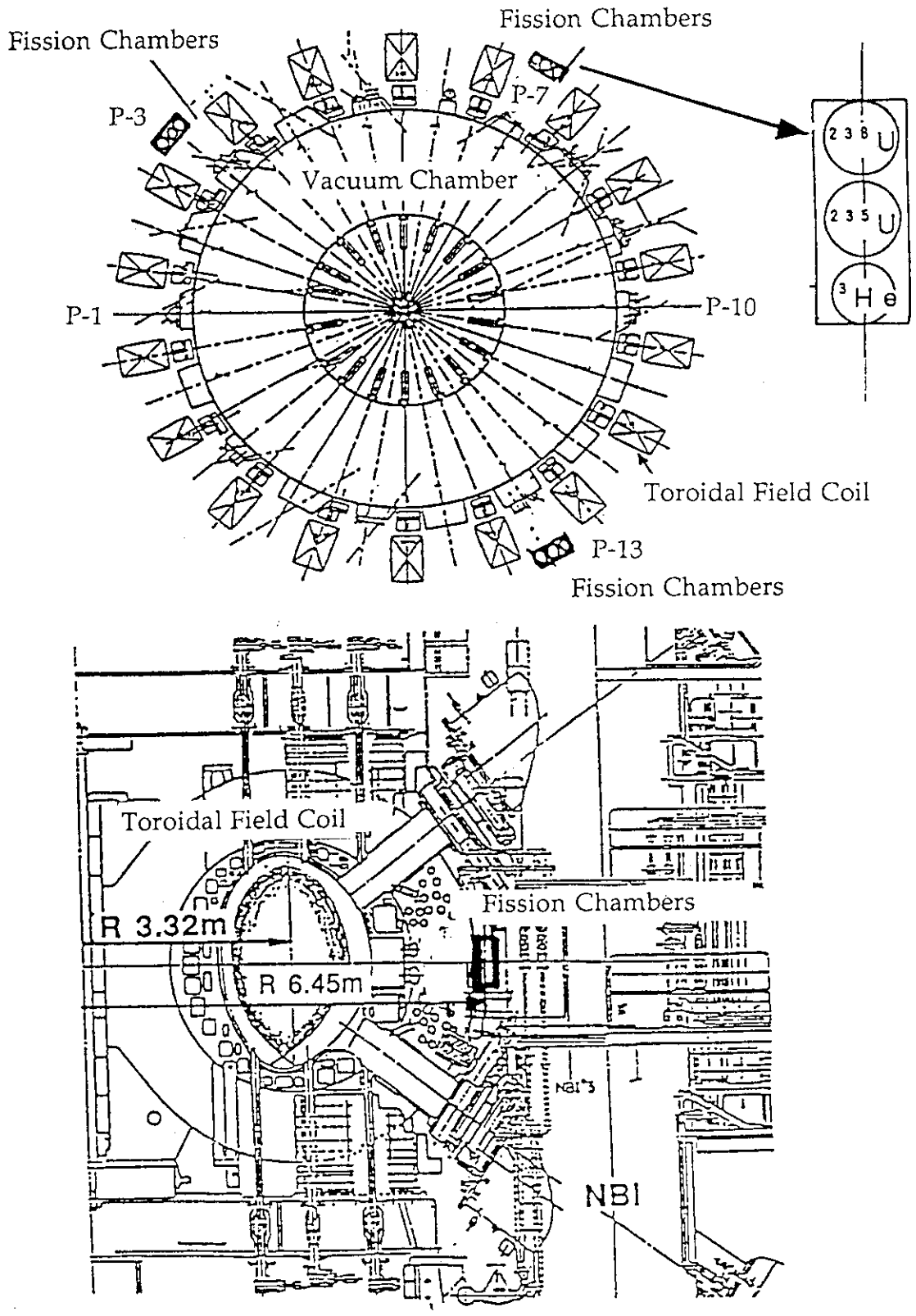

Fig. 1 Arrangement of the neutron detectors on the JT-60 Upgrade

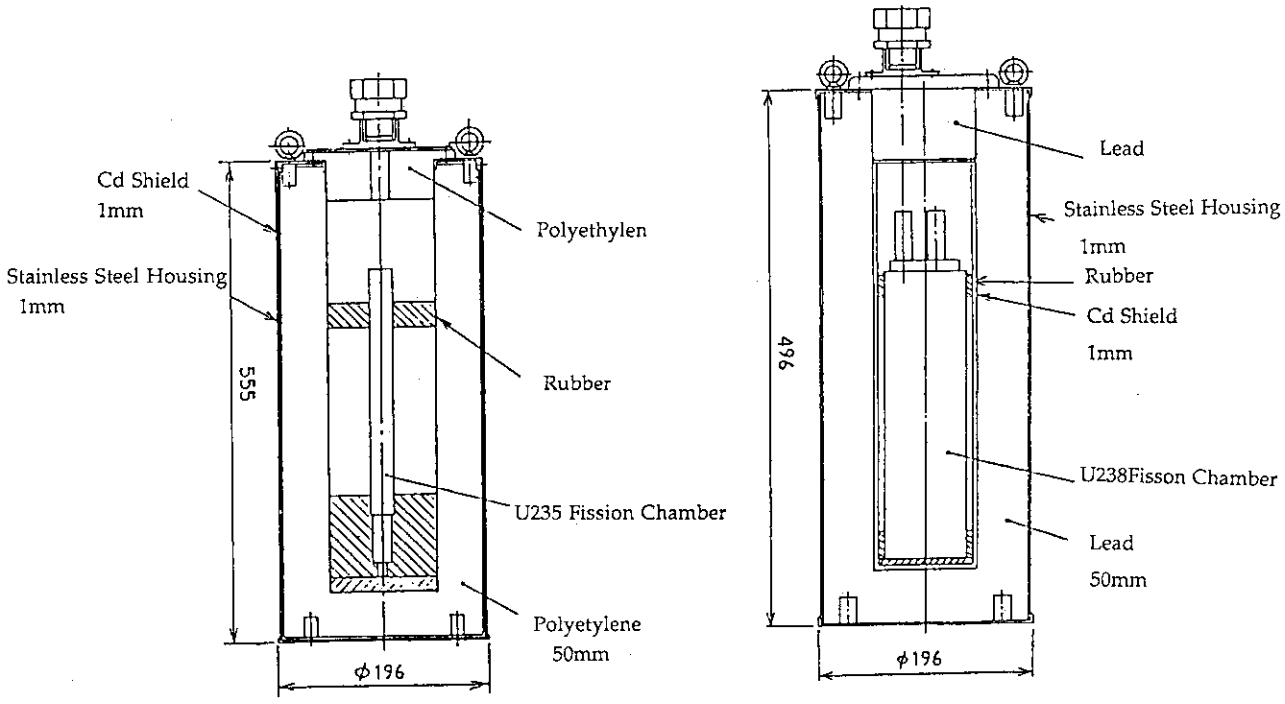

Fig. 2 Schematics of the ^{235}U and ^{238}U detectors

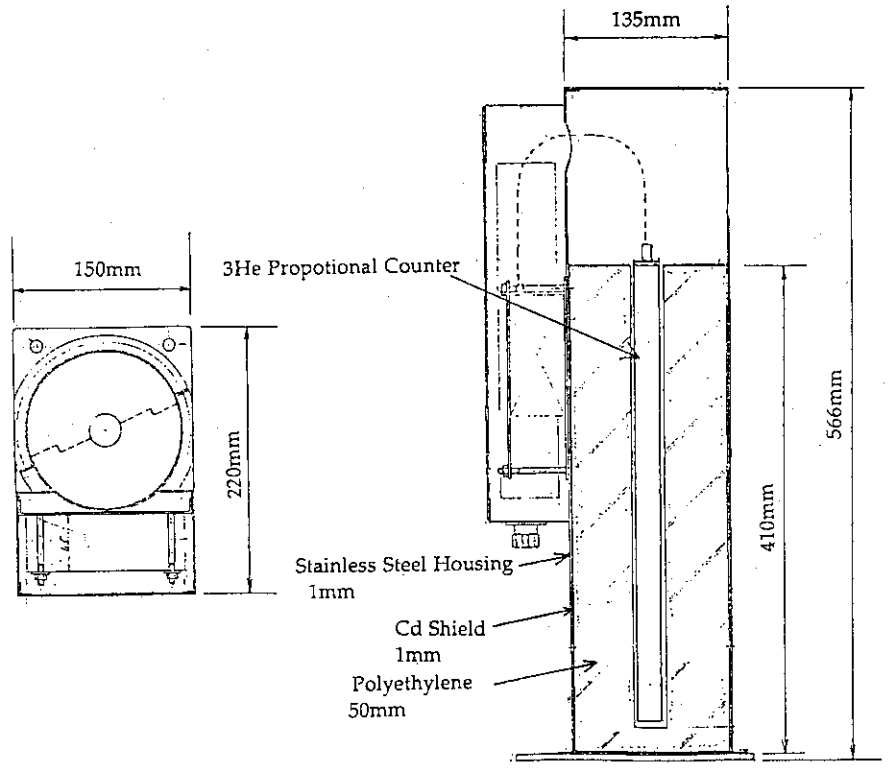

Fig. 3 Schematics of the ^{3}He proportional counter

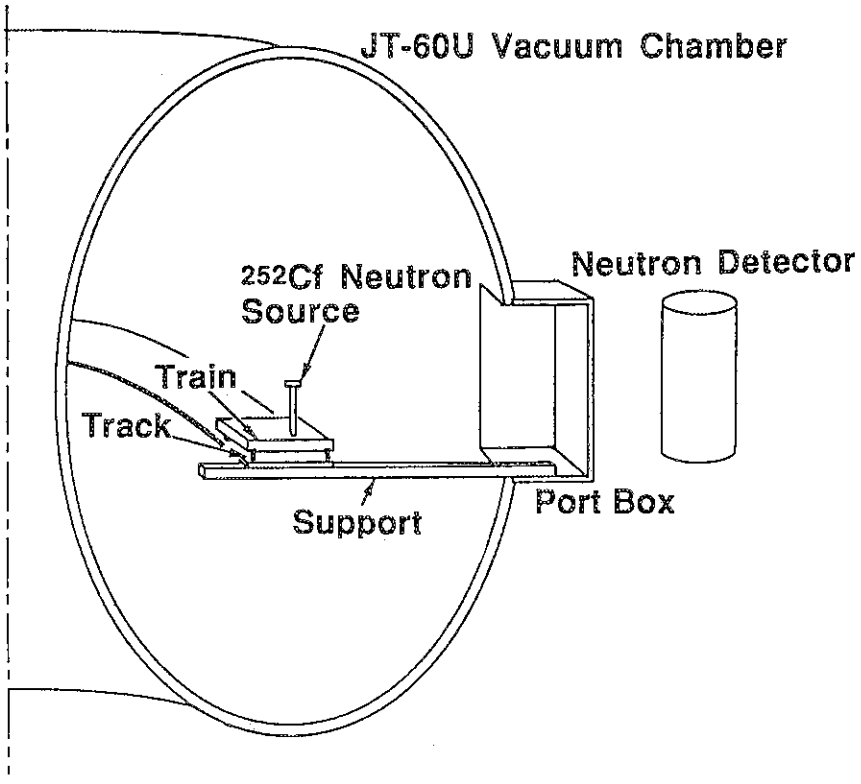

Fig. 4 Schematics of the source transfer system in the vacuum vessel of JT-60 Upgrade

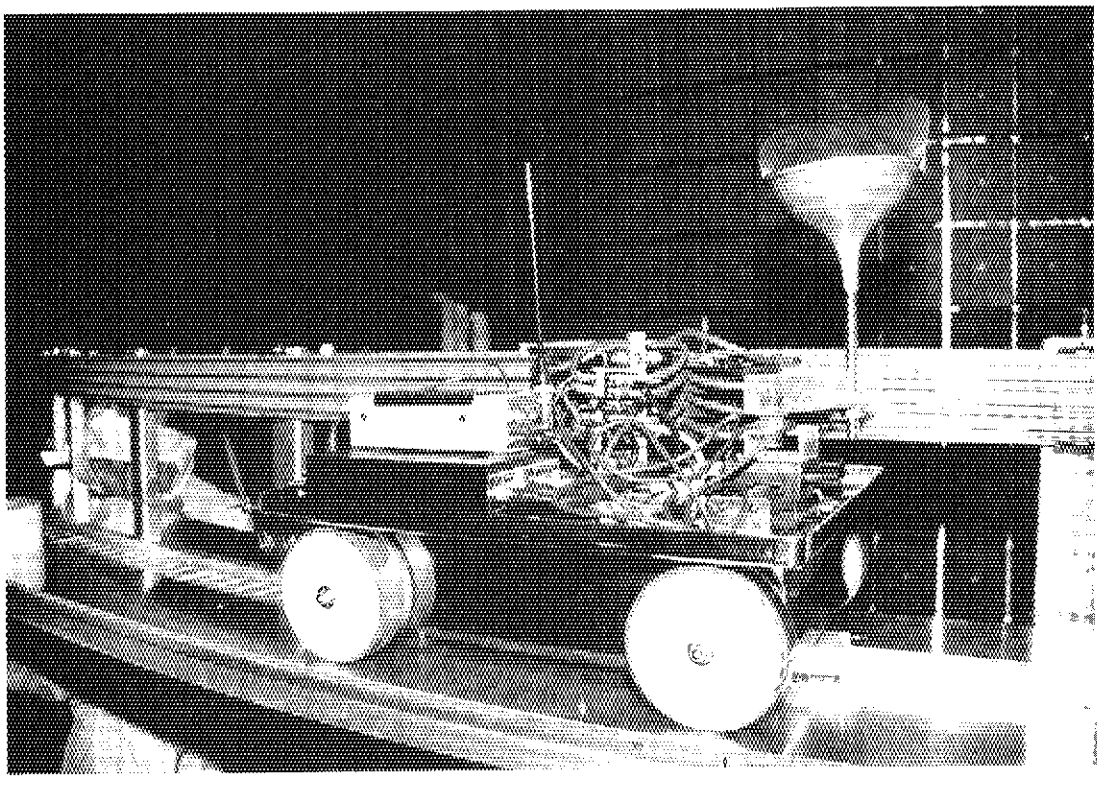

Fig. 5 Photograph of the source transfer system consisted of 'train and track'

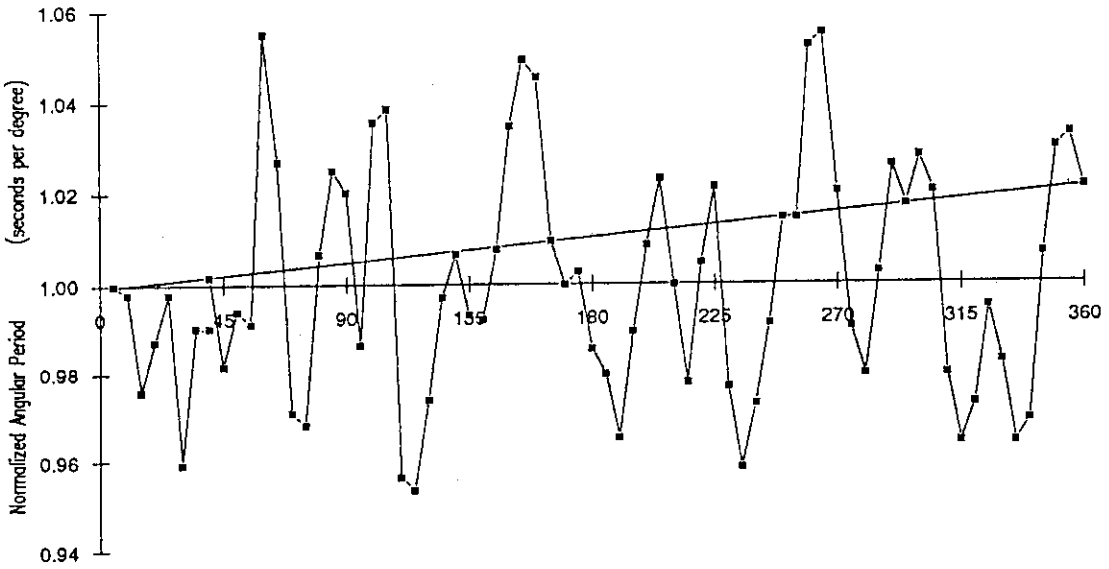

Fig. 6 Normalized Angular Period (seconds per degree, the average being 2.072 secs per degree) vs toroidal angle of the calibration train

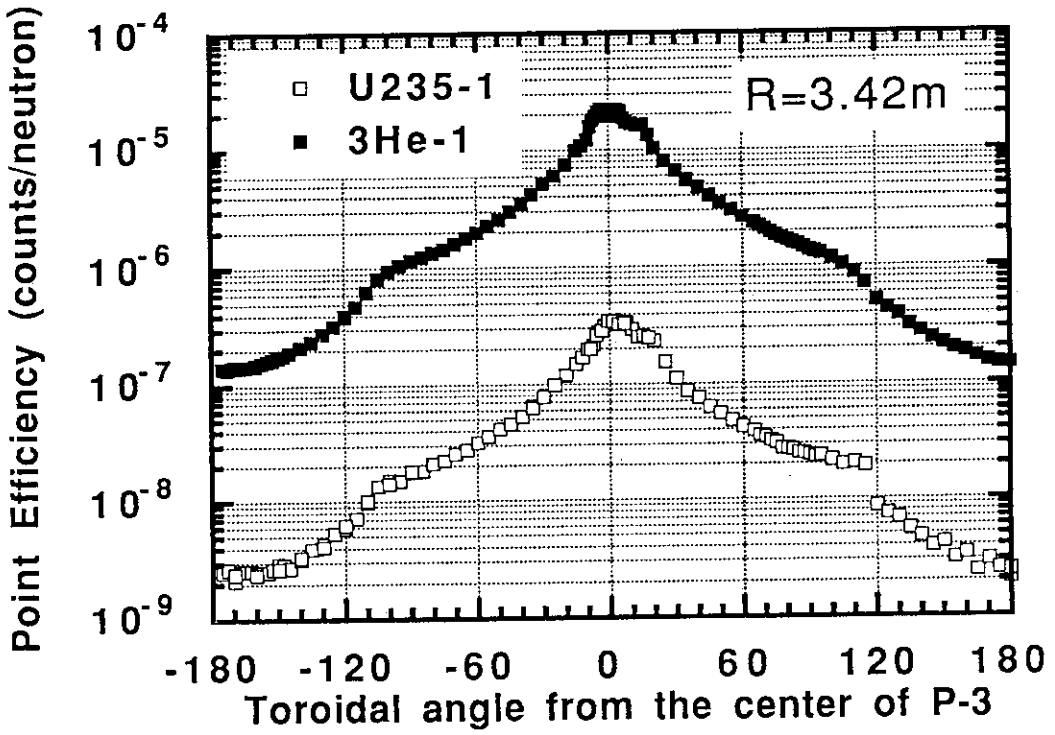

Fig. 7 Point efficiencies for ^{235}U and ^{3}He detectors in Bay P-3 versus toroidal angle

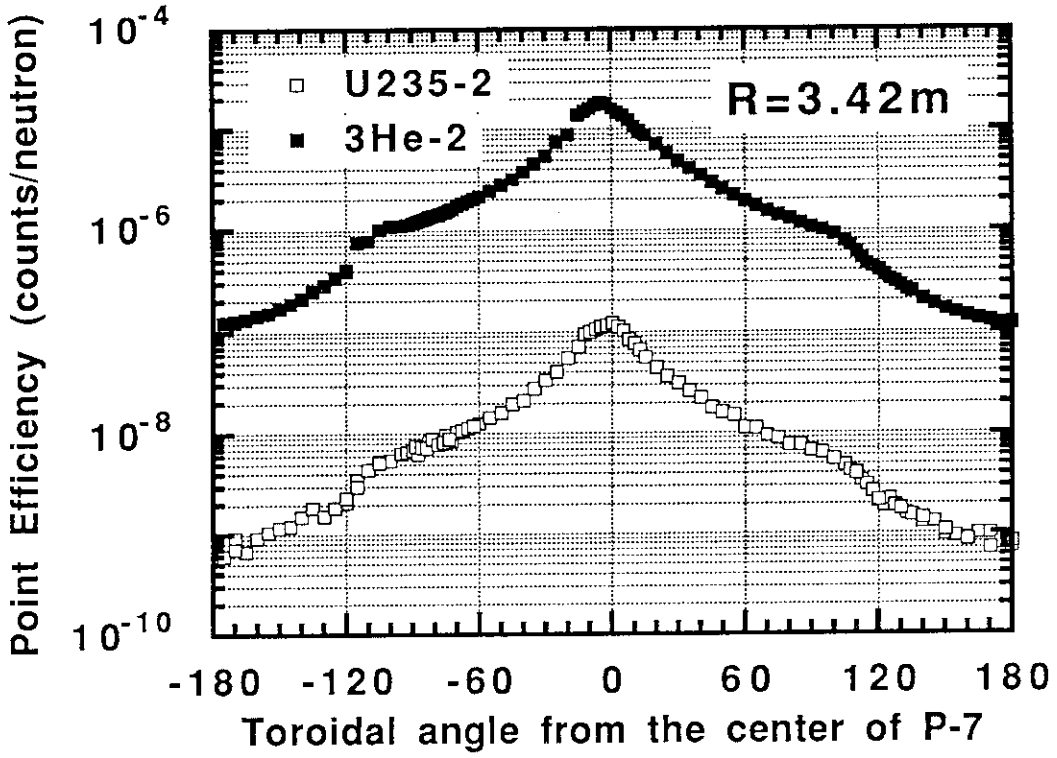

Fig. 8 Point efficiencies for ^{235}U and ^{3}He detectors in Bay P-7 versus toroidal angle

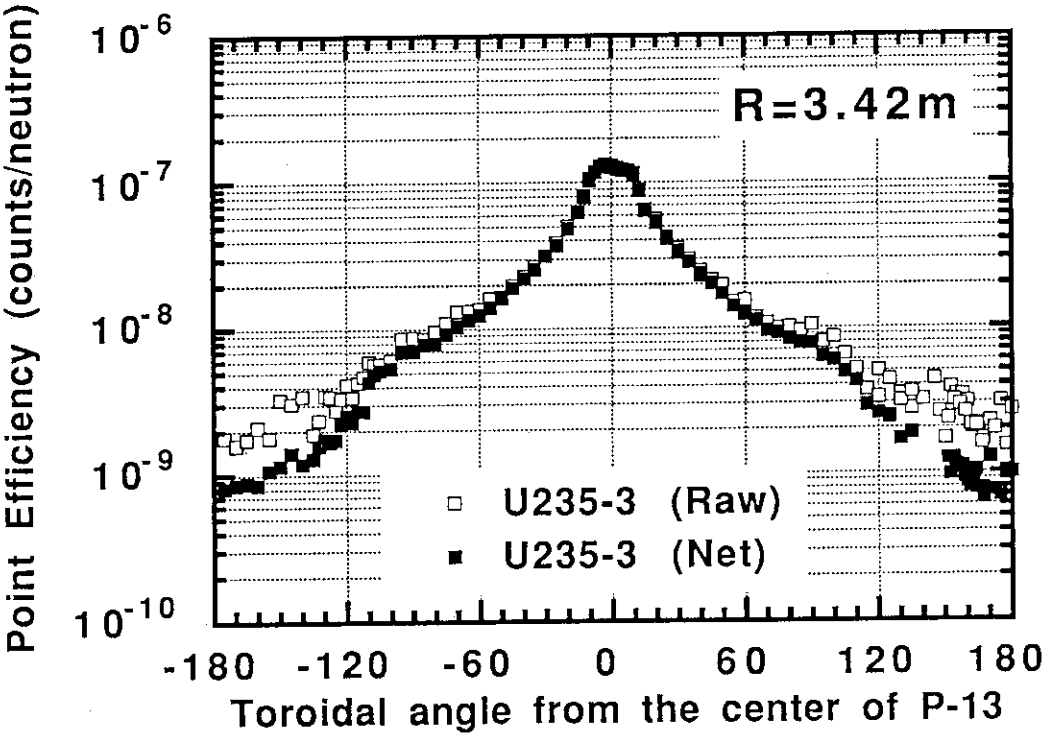

Fig. 9 Point efficiency for Bay P-13 ^{235}U detector versus toroidal angle, comparing "Raw" measured counts and "Net" counts with noise subtracted

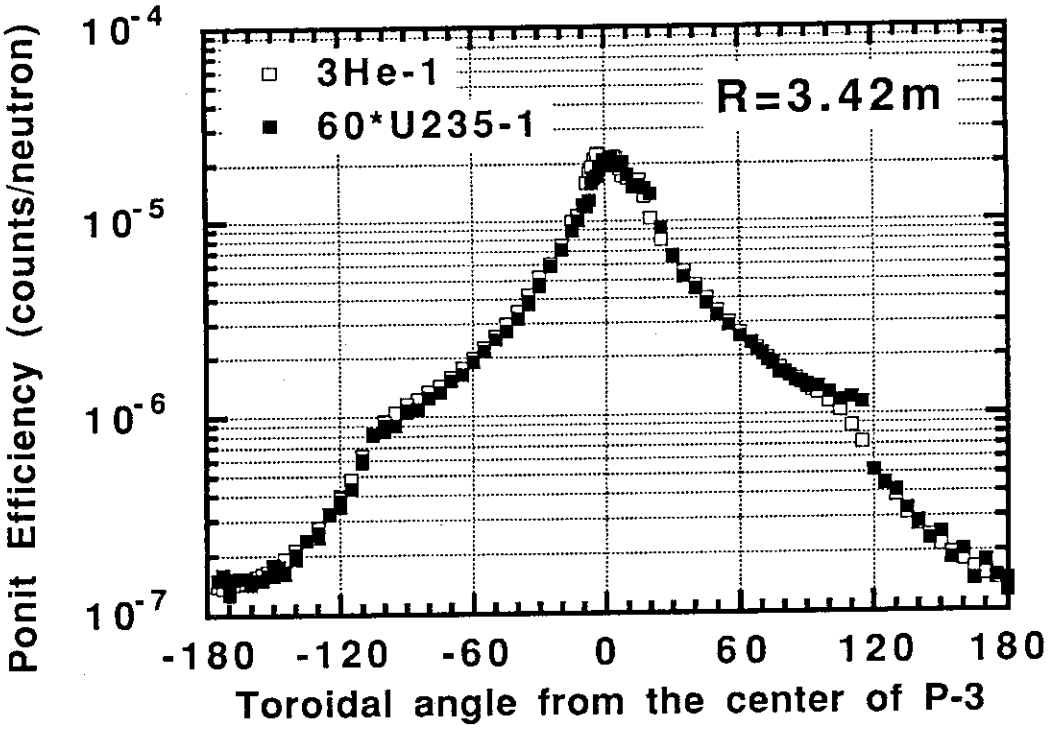

Fig. 10 Point Efficiency (log scale) vs toroidal angle for two detectors in Bay P-3. The data for the ^{235}U detector have been multiplied by 60

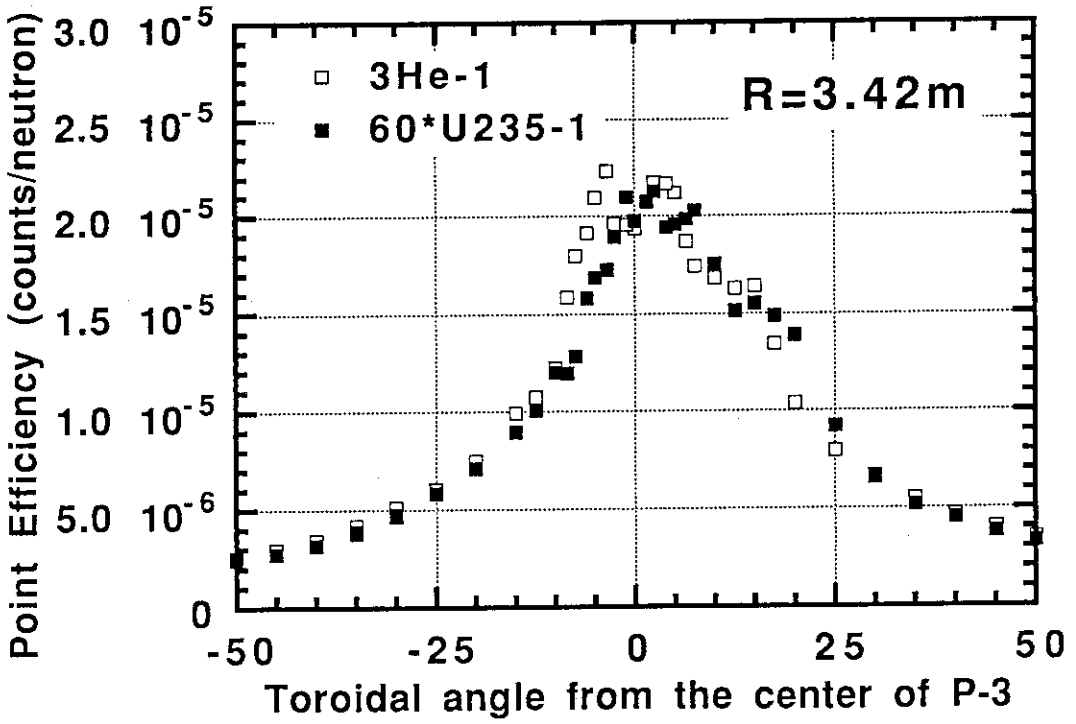

Fig. 11 Same as Figure 10, but on linear vertical scale and reduced angular axis. Notice the structure in the data, and the angular shift between the detectors

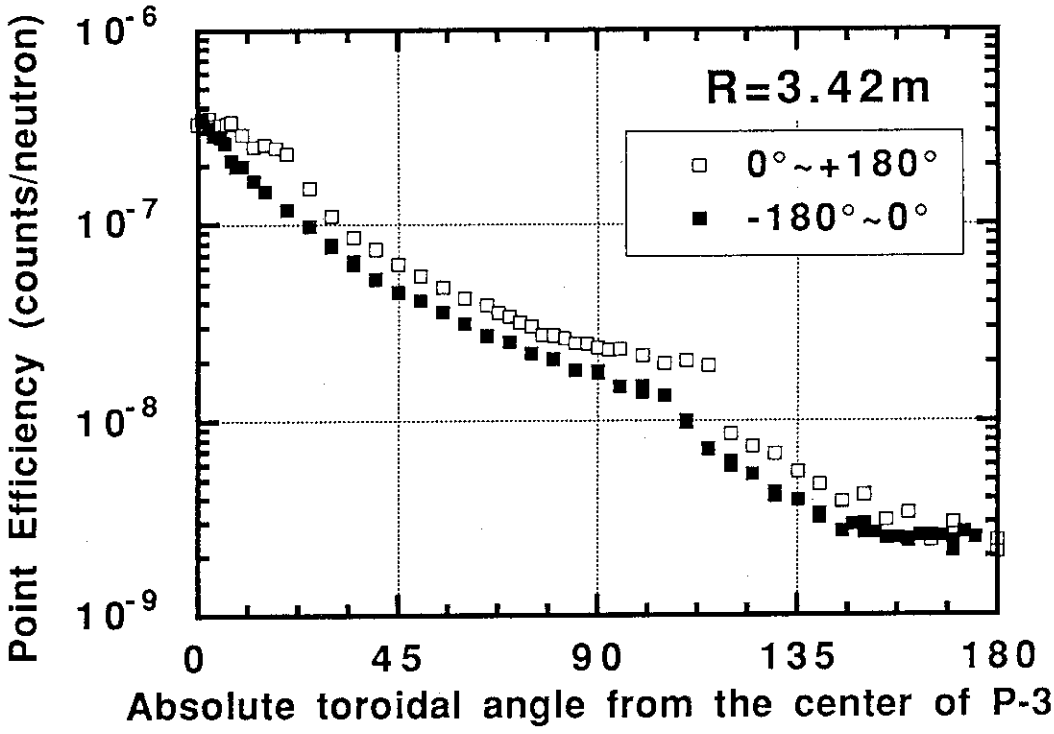

Fig. 12 ^{235}U point efficiency vs absolute value of the toroidal angle

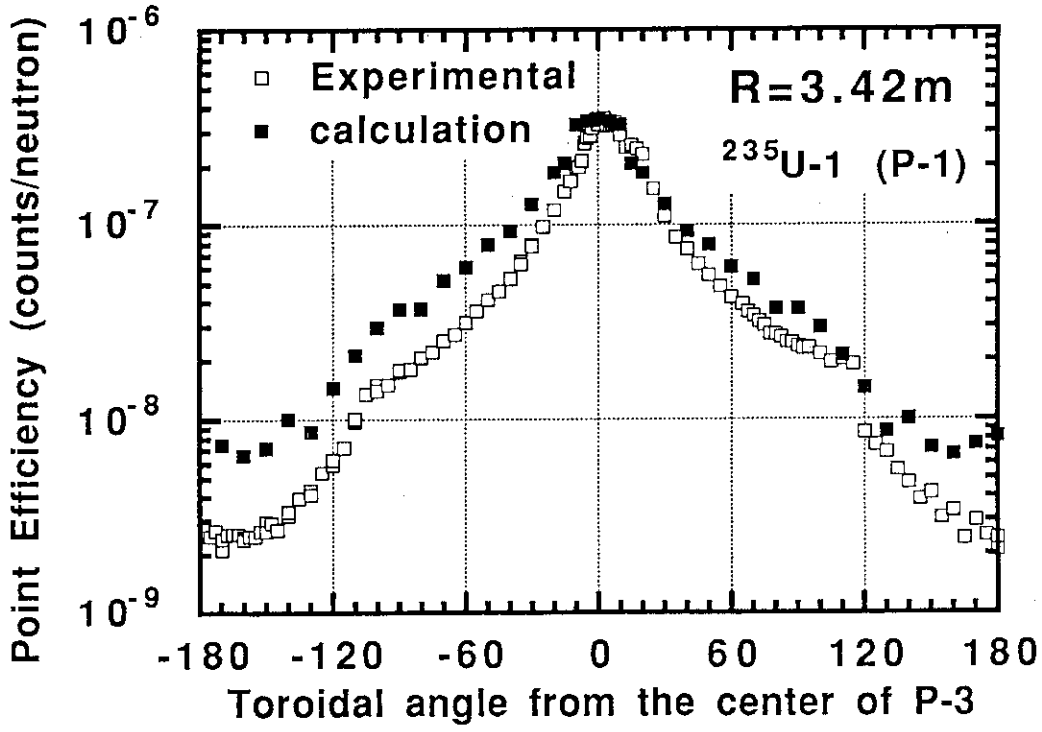

Fig. 13 Comparison of the point efficiencies between the experiment and the MCNP calculation for the ^{235}U-1 of Bay P-3

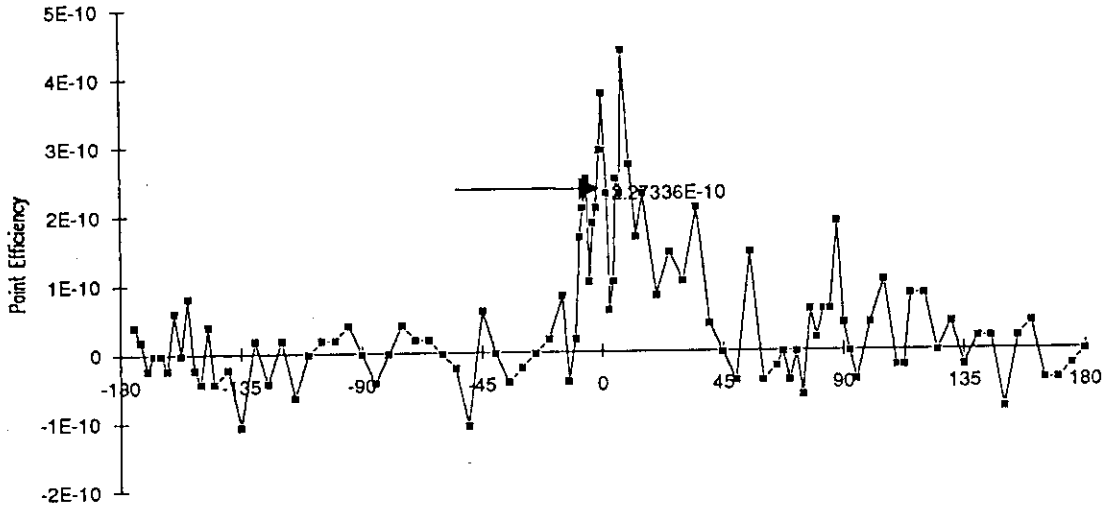

Fig. 14 ^{238}U point efficiency, calculated by subtracting a background of 154 counts per 1000 seconds, vs toroidal angle. The arrow and value label a single data point taken for 10000 seconds

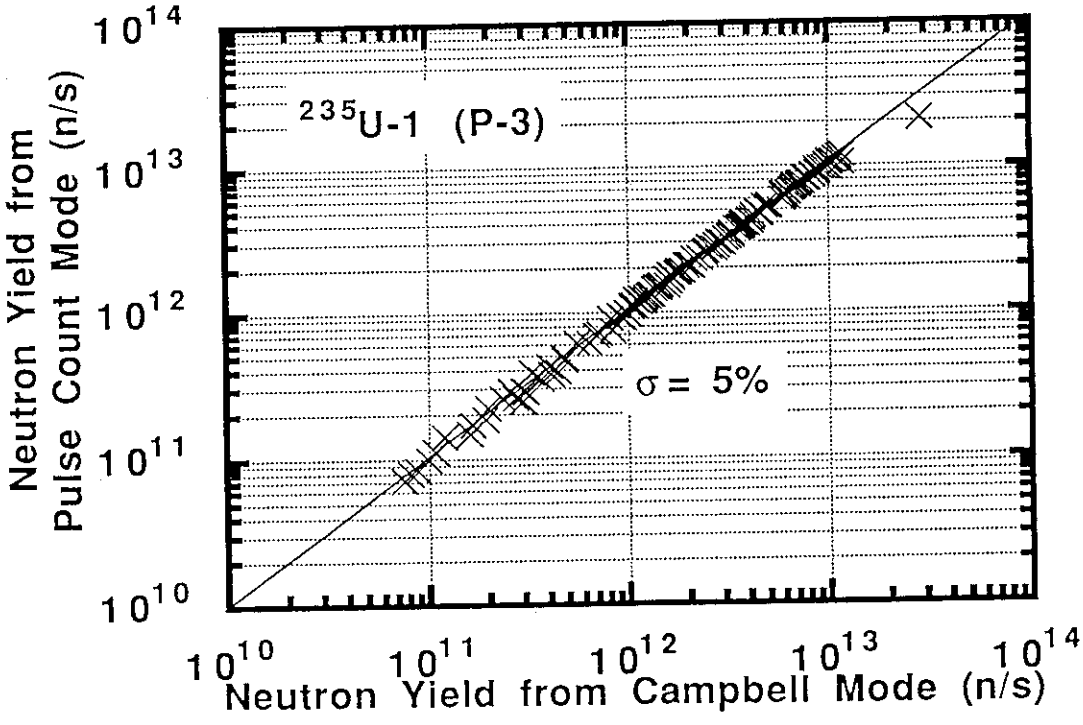

Fig. 15 Cross calibration of the Bay P-3 ^{235}U detector from the pulse counting mode to the Campbell mode